

Large deflections of non-prismatic nonlinearly elastic cantilever beams subjected to non-uniform continuous load and a concentrated load at the free end

Miha Brojan · Matjaz Cebon · Franc Kosel

Received: 17 June 2011 / Revised: 19 December 2011 / Accepted: 20 December 2011

©The Chinese Society of Theoretical and Applied Mechanics and Springer-Verlag Berlin Heidelberg 2012

Abstract This work studies large deflections of slender, non-prismatic cantilever beams subjected to a combined loading which consists of a non-uniformly distributed continuous load and a concentrated load at the free end of the beam. The material of the cantilever is assumed to be nonlinearly elastic. Different nonlinear relations between stress and strain in tensile and compressive domain are considered. The accuracy of numerical solutions is evaluated by comparing them with results from previous studies and with a laboratory experiment.

Keywords Large deflections · Non-prismatic beams · Combined loading · Generalized Ludwick constitutive law · Material and geometrical nonlinearity

1 Introduction

In many areas of modern engineering designers use slender structural elements made from materials for which a nonlinearly elastic model is a reasonable approximation. Therefore the geometry and the composition of the elements often require nonlinear analysis of the given problem. There are a number of contributions that can be found in the literature on this topic. Those, closest to our interest are listed and briefly discussed below.

For example, large deflections of a prismatic cantilever beam made of Ludwick type material under a combined loading consisting of a uniformly distributed load and a vertical concentrated force at the free end have been studied by Lee [1] and Eren [2]. Baykara et al. [3] investigated the effect of bimodulus material behavior on the horizontal and vertical deflections of the free end of a thin cantilever beam which is subjected to an end moment. Brojan [4] analyzed

bending of non-prismatic beams made of Ludwick type material with different stress–strain relationships in tension and compression. An analytical solution in terms of infinite series was found for the case when the nonlinear stress–strain relationship in tensile and compressive domain is identical. A similar problem was examined by Shatnawi and Al-Sadder in Ref. [5]. Recently a generalized version of Ludwick’s rheological model has been suggested to improve the non-physical behavior of the classical Ludwick type material at small strains in a study done by Jung and Kang [6] and discussed by Brojan et al. in Ref. [7]

A more comprehensive list of publications on some other configurations of nonlinearly elastic planar beams can be found in Ref. [7]. The same article includes a useful comparison between Hooke’s, Ludwick’s and generalized Ludwick’s model, i.e. the models which can be relatively easily and effectively used in engineering practices.

The main focus of this paper is on the examination of large deflections of non-prismatic, nonlinearly elastic cantilever beams subjected to a combined loading which consists of a non-uniformly distributed continuous load and a concentrated load at the free end.

2 Formulation of the problem

A slender, non-prismatic cantilever beam subjected to a non-uniformly distributed continuous load and a concentrated load at the free end of the beam is considered in this study. The origin of the Cartesian (x, y) coordinate system is placed at the clamped end and the x -axis coincides with the longitudinal axis of the undeformed beam. The length of the longitudinal axis of the initially straight cantilever is L .

Variable s , $0 \leq s \leq L$, Fig. 1, denotes a curvilinear coordinate along the neutral axis measured from the fixed end of the beam and $\theta(s)$ represents the angle between the positive direction of the x -axis and the tangent to the neutral axis at point s . The beam has a rectangular cross-section of variable width $o(s)$ and variable height $h(s)$, which are defined by the

M. Brojan (✉) · M. Cebon · F. Kosel
Laboratory for Nonlinear Mechanics,
Faculty of Mechanical Engineering, University of Ljubljana,
Askerceva 6, SI-1000 Ljubljana, Slovenia
e-mail: miha.brojan@fs.uni-lj.si

following equations

$$o(s) = o_e \left(\frac{1-a}{L}s + a \right)^p, \quad h(s) = h_e \left(\frac{1-b}{L}s + b \right)^r, \quad (1)$$

where a, b, p, r are given shape coefficients and o_e, h_e indicate the width and height of the beam at the free end. The distributed load is described with a similar function

$$q(s) = q_e \left(\frac{1-c}{L}s + c \right)^t. \quad (2)$$

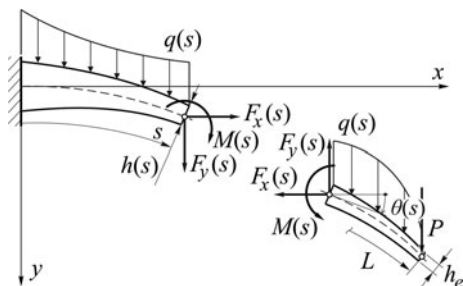


Fig. 1 Non-prismatic cantilever beam subjected to a combined loading

The beam is composed of a nonlinearly elastic material with a different material behavior in tensile and compressive domain.

A relatively simple expression which is frequently used to describe nonlinear material properties is represented by the Ludwick's law, $\sigma(\varepsilon) = \text{sign}(\varepsilon)E|\varepsilon|^{1/k}$, where elements σ, ε, E and k are stress, strain, and two material constants, respectively. This expression, although mathematically compliant, demonstrates a non-physical behavior of the material when $\varepsilon \rightarrow 0$, which makes it unsuitable for linearization at small strains. Jung and Kang [6] therefore suggested an improvement of this formula, a generalized Ludwick's law in which an additional material parameter is used. This particular material model is also utilized in the present study, so that

$$\sigma(\varepsilon) = \begin{cases} E_T((\varepsilon + \varepsilon_{0T})^{1/n} - \varepsilon_{0T}^{1/n}), & \text{for } \varepsilon \geq 0, \\ -E_C((|\varepsilon| + \varepsilon_{0C})^{1/m} - \varepsilon_{0C}^{1/m}), & \text{for } \varepsilon < 0. \end{cases} \quad (3)$$

Many real materials with nonlinear properties can be described by this model, e.g. natural rubber in the domain of smaller strain where elastic component is dominant compared to viscous component.

Along with assumptions stated above we also impose that the material is incompressible; that shear stresses in the beam are negligible in comparison with normal stresses because the length-height ratio of the beam is large; that cross-sections which are perpendicular to the neutral axis before deformation, remain plain and perpendicular to the neutral axis in the deformed state of the beam and do not change their shape and area.

3 Governing equations

According to Fig. 1, equations of static equilibrium of internal forces in the direction of the Cartesian coordinates give

$$F_x(s) = 0, \quad (4)$$

$$F_y(s) = \int_s^L q(\sigma)d\sigma + P.$$

Furthermore, from equilibrium of an infinitesimal element of the deflected beam, cf. Fig. 2, geometrical relation $\cos \theta(s) = dx/ds$ and Eq. (4), we can deduce

$$M'(s) + F_y(s) \cos \theta(s) = 0, \quad (5)$$

where “'” denotes differentiation with respect to variable s .

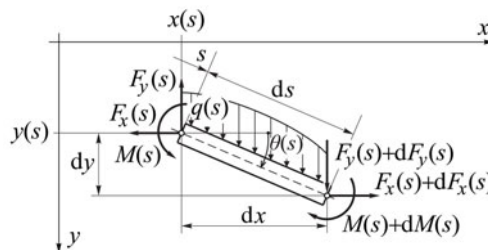


Fig. 2 An infinitesimal element of the deflected beam

Given that the cross-section, the model of deformation of the beam and the stress–strain function of the material are defined we can formulate an expression linking the inner bending moment to the curvature of the neutral axis.

Figure 3 shows an infinitesimal element of the beam in the deformed state and the nonlinear distribution of normal stress over the cross-section. The normal strain is given by expression $\varepsilon = \rho(s)^{-1}z$, where $\rho(s)$ is the radius of curvature of the neutral axis, and $\rho(s)^{-1} = \theta'(s)$.

The inner bending moment acting on an arbitrary cross-section of the beam can be expressed with normal stress as $M(s) = \int_A \sigma z dA$. By considering the relation between stress and strain equation (3) and the normal strain-curvature expression mentioned above, we can derive

$$M(s) = E_T o(s) \left[(\theta(s)h_T(s) + \varepsilon_{0T})^{1+1/n} \times \frac{n(1+n)\theta(s)h_T(s) - \varepsilon_{0T}n^2}{(1+2n)(1+n)\theta(s)^2} + \frac{\varepsilon_{0T}^{2+1/n}n^2}{(1+n)(1+2n)\theta(s)^2} - \frac{\varepsilon_{0T}^{1/n}h_T(s)^2}{2} \right] + E_C o(s) \left[(\theta(s)h_C(s) + \varepsilon_{0C})^{1+1/m} \times \frac{m(1+m)\theta(s)h_C(s) - \varepsilon_{0C}m^2}{(1+2m)(1+m)\theta(s)^2} + \frac{\varepsilon_{0C}^{2+1/m}m^2}{(1+m)(1+2m)\theta(s)^2} - \frac{\varepsilon_{0C}^{1/m}h_C(s)^2}{2} \right]. \quad (6)$$

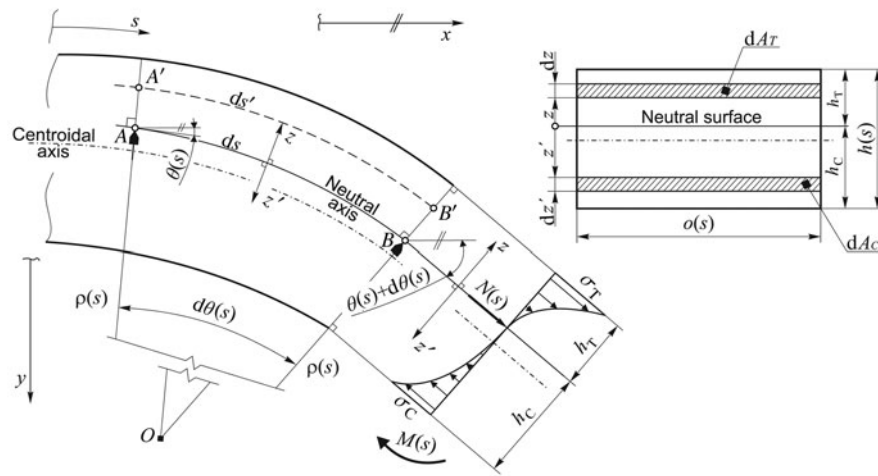


Fig. 3 Deformation and normal stresses on a cross-section of the deformed beam

Since the stress–strain relation is different in tension and compression, the neutral axis does not coincide with the centroidal axis. As the beam deflects the component normal to the beam’s cross section of the F_y force becomes more important. Large axial stresses are induced along the beam and the moment’s arm along the beam is reduced significantly when the applied end load becomes very large. But the influence of the inner axial force on the deformation of slender beams can readily be neglected as shown for our case in the Appendix. Values of $h_T(s)$ and $h_C(s)$, see Fig. 3, can therefore be determined by considering that the deformation of the beam is caused only by the inner bending moment. It then follows that the resultant in terms of force of normal stresses in any cross-section equals zero, i.e. $N(s) = \int_A \sigma dA = 0$, from which we can find

$$\begin{aligned}
 E_T \left\{ \frac{n}{1+n} \theta(s)^{-1} [(\theta(s)h_T(s) + \epsilon_{0T})^{(1+n)/n} - \epsilon_{0T}^{(1+n)/n}] \right. \\
 \left. - \epsilon_{0T}^{1/n} h_T(s) \right\} \\
 = E_C \left\{ \frac{m}{1+m} \theta(s)^{-1} [(\theta(s)h_C(s) + \epsilon_{0C})^{(1+m)/m} - \epsilon_{0C}^{(1+m)/m}] \right. \\
 \left. - \epsilon_{0C}^{1/m} h_C(s) \right\}. \tag{7}
 \end{aligned}$$

It can be noted from Fig. 3 that

$$h_T(s) + h_C(s) = h(s). \tag{8}$$

Finally by using Eqs. (5) and (6), the governing differential equation of the problem can be deduced in the following form

$$\begin{aligned}
 \left\{ E_T n \left[\frac{n \epsilon_{0T} \beta_T (1 + 1/n)}{(1+n)(1+2n)} + \frac{h_T(s) \alpha_T(s)^{1+1/n}}{1+2n} \theta'(s) \right. \right. \\
 \left. \left. - \frac{\epsilon_{0T}^{1/n} h_T(s)^2}{2n} \theta'(s)^2 \right] + E_C m \left[\frac{m \epsilon_{0C} \beta_C (1 + 1/m)}{(1+m)(1+2m)} \right. \right. \\
 \left. \left. + \frac{h_C(s) \alpha_C(s)^{1+1/m}}{1+2m} \theta'(s) - \frac{\epsilon_{0C}^{1/m} h_C(s)^2}{2m} \theta'(s)^2 \right] \right\} \frac{o'(s)}{\theta'(s)^2} \\
 - \left\{ \frac{E_T}{1+2n} \left[\frac{2n^2 \epsilon_{0T}^2 \beta_T (1/n)}{1+n} + \frac{2n \epsilon_{0T} h_T(s) \alpha_T(s)^{1/n}}{1+n} \theta'(s) \right. \right. \\
 \left. \left. - h_T(s)^2 \alpha_T(s)^{1/n} \theta'(s)^2 \right] + \frac{E_C}{1+2m} \right. \\
 \left. \times \left[\frac{2m^2 \epsilon_{0C}^2 \beta_C (1/m)}{1+m} + \frac{2m \epsilon_{0C} h_C(s) \alpha_C(s)^{1/m}}{1+m} \theta'(s) \right. \right. \\
 \left. \left. - h_C(s)^2 \alpha_C(s)^{1/m} \theta'(s)^2 \right] \right\} o(s) \frac{\theta''(s)}{\theta'(s)^3} \\
 - [E_T \beta_T (1/n) h_T(s) h_T'(s) + E_C \beta_C (1/m) h_C(s) h_C'(s)] o(s) \\
 + F_y \cos \theta(s) = 0, \tag{9}
 \end{aligned}$$

where two auxiliary functions have been introduced,

$$\begin{aligned}
 \alpha(s) &= \epsilon_0 + h(s) \theta'(s), \\
 \beta(p) &= \epsilon_0^p - \alpha^p. \tag{10}
 \end{aligned}$$

Expressions for the derivatives of the functions h_T and h_C in the above differential equation can be obtained from Eqs. (7) and (8). The geometry of the problem discussed in this article also requires

$$\begin{aligned}
 \theta(s=0) &= 0, \\
 \theta'(s=L) &= 0. \tag{11}
 \end{aligned}$$

4 Numerical solutions

The solution of the system of differential equations (7)–(11) is found by using a Runge–Kutta–Nyström integration method and implicitly applying the Newton–Raphson iterative method to solve Eq. (7). The value of the unknown function θ' at $s = 0$, is found by employing a one-parameter shooting method. After obtaining the numerical solution for $\theta(s)$, the Cartesian coordinates of the points along neutral axis can be determined from the geometrical relations which follow from Fig. 2, i.e. $\sin \theta(s) = dy/ds$, $\cos \theta(s) = dx/ds$, or, respectively, $x(s) = \int_0^s \cos \theta(t)dt$, $y(s) = \int_0^s \sin \theta(t)dt$, together with boundary conditions $x(s = 0) = 0$ and $y(s =$

Table 2 Geometrical properties and load parameters for Examples 1 and 2

#	o/mm	L/mm	h_e/mm	a	r	$q_0/(N \cdot mm^{-1})$	b	t
1	39.3	180.0	9.8	2.0	2.0	8.347×10^{-2}	2.0	1.0
2	39.3	180.0	9.8	0.11	0.5	4.174×10^{-3}	0.5	4.0

In the first example a narrowing profile of the cantilever is considered while the continuous load is chosen to be of a trapezoidal shape. As a result of the much larger rigidity of the beam near the fixed end than at the free end, while angle θ at the free end reaches values close to $\pi/2$, which is the maximum we can achieve at given load directions, the curvature of the beam at the fixed end remains relatively small, cf. Fig. 4. Also as a consequence of the variability of the height of the cross section, the location of the largest curvature does not coincide with the location of the largest inner bending moment, which is at the fixed end.

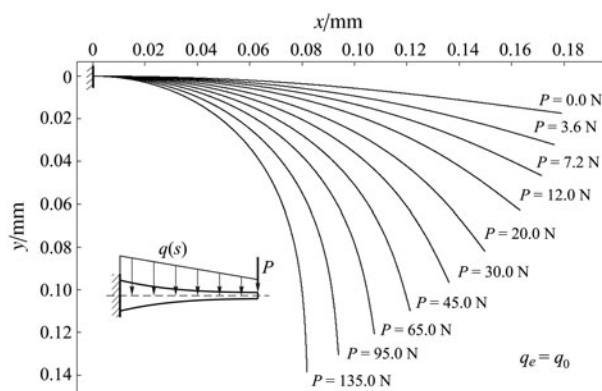


Fig. 4 Deflections of the neutral axis for Example 1

In Example 2 a widening profile of the cantilever is considered while the configuration of the continuous load is non-linear and increasing from the fixed to the free end. Figure 5 shows characteristically different deflected profiles compared with those in Example 1. All the relevant deformation of the beam seems to be concentrated near the fixed end while the rest of the beam remains practically straight. The

$y) = 0$.

Two examples with the same configuration and material constants but different shape coefficients are presented to illustrate the influence of the profile of the beam on the deflected shape of the neutral axis. Material parameters, geometrical properties and load parameters for Examples 1 and 2 are given in Tables 1 and 2, respectively.

Table 1 Material parameters

E_T/MPa	E_C/MPa	n	m	ϵ_{0T}	ϵ_{0C}
1.73	5.32	1.619	1.213	0.001	0.001

maximum curvature of the beam is in this case clearly located at the fixed end since both the thinnest cross section and the largest bending moment are situated at this point.

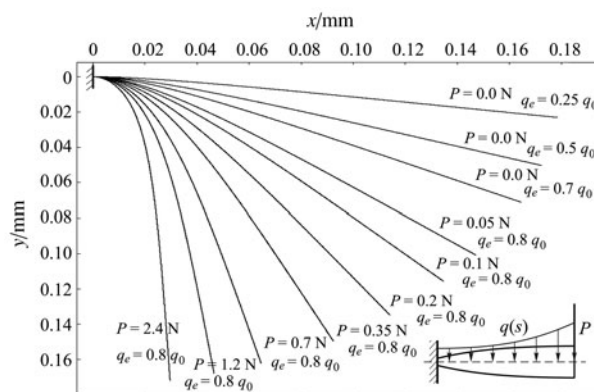


Fig. 5 Deflections of the neutral axis for Example 2

5 Experiment

The experiment was carried out on a prismatic beam subjected to gravitation, i.e. self weight which represents a uniform continuous load, and a vertical force at the free end, see Fig. 6.

A special type of vulcanized rubber which has a relatively small viscous component at smaller strain (obtained from Savatech d.o.o. rubber company) was chosen to be the material of the beam. During the experiment the positions of several selected points on the upper surface of the beam, Fig. 6, were being measured while different weights were being applied at the free end of the beam, Fig. 7.

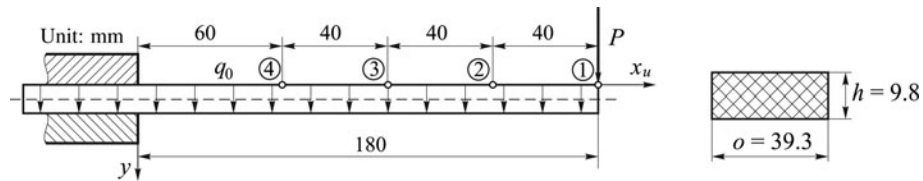


Fig. 6 Experimental configuration of the beam



Fig. 7 Measurement of deflections of the beam

The results of these measurements can be found in Table 3. Geometrical properties together with the loads on the experimental configuration of the beam are listed in Table 4.

The experimental results and the results obtained using the method of solution presented above can not be directly compared since the positions of selected experimental points are not located on the neutral axis. To determine the displacement of points on the upper surface of the beam, the following geometrical relations have to be considered

$$\begin{aligned}
 y_u(s) &= y(s) - h_T(s) \cos(\theta(s)), \\
 x_u(s) &= x(s) + h_T(s) \sin(\theta(s)).
 \end{aligned}
 \tag{12}$$

Table 3 Results of the measurements of deflections

#	P/N	Point 1		Point 2		Point 3		Point 4	
		x_u /mm	y_u /mm						
1	0.0000	179	16	139	12	99	8	60	4
2	0.1962	176	27	138	20	99	12	60	6
3	0.4905	173	49	135	34	98	21	59	10
4	0.6867	168	63	133	45	97	27	59	12
5	0.9810	160	80	127	58	95	35	58	16
6	1.4715	147	103	119	73	90	45	58	20
7	1.9620	135	115	112	84	86	53	57	24
8	2.9430	118	134	98	99	78	64	54	30
9	3.9240	103	143	90	108	73	70	53	34
10	4.9050	91	152	82	114	67	76	50	38

Table 4 Geometrical properties and load parameters for the experimental configuration of the beam

o /m	L /mm	h_c /mm	a	r	q_c /(N · mm ⁻¹)	b	t				
39.3	180.0	9.8	1.0	0.0	4.174×10^{-3}	1.0	0.0				
#	1	2	3	4	5	6	7	8	9	10	
P/N	0.0000	0.1962	0.4905	0.6867	0.9810	1.4715	1.9620	2.9430	3.9240	4.9050	

The stress–strain curve of the material of the beam used in the calculations was measured using a Zwick/Roell Z050 testing machine. Mechanical tests were carried out at temperature 24 °C, approx. 55 % air humidity and at deformation rate of 25 mm/min. The accuracy of the testing ma-

chine was 0.4 % for the force measurements and 0.02 % for measurement of the displacement. Standard sized and shaped specimens were used in compressive and tensile tests, Fig. 8. The specimens were subjected to cyclic loading to about 40 % strain until the material reached a steady-state re-

sponse, which was approx. after 5 cycles. Although it is well known that mechanical behavior of rubber is generally time-dependent, this characteristic is neglected and only a steady-state response is taken into account. Therefore, the instantaneous response of the beam is considered which means that measurements of the beam's deflections, see Table 3, had to be taken in the first 10–20 s of the loading. In time deflections increased as expected. The results of measurements of the material properties are depicted in Fig. 8 where non-linear behavior is evident in both tensile and compressive domain. The largest strain obtained from the numerical solution of experimental cases is approximately 0.16 in tension and 0.12 in compression and in both cases it remains within the region where a satisfactory approximation of the experimental stress–strain curve is achieved. Material constants, presented in Table 1, of the generalized Ludwick rheological law were determined from the experimental data by the least square method.

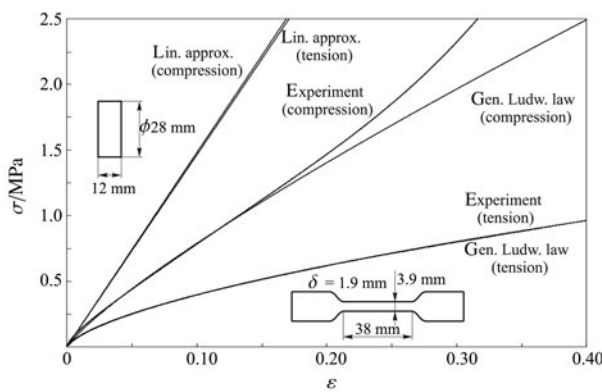


Fig. 8 Experimental and theoretical stress–strain curves

In Fig. 9 experimental and numerical results for the case of approximating the stress–strain curve with the generalized Ludwick law are shown. In this case a good agreement between numerical and experimental results is found. As expected from the measurements of the stress–strain curve of the material, good results are achieved by considering different stress–strain relation of the material in tension and compression and using an adequate rheological model. Slightly less accurate results which are not presented in this study were also obtained by using the classical Ludwick law. In addition, the results obtained by simplifying our model to the model set up by Lee [1] and Eren [2] are in perfect agreement.

As already mentioned in the introduction, although Ludwick's model is mathematically compliant, it demonstrates a non-physical behavior of the material when $\epsilon \rightarrow 0$, which makes it unsuitable for linearization at small strains. On the other hand, the generalized Ludwick law can be linearized at small strains. Namely, from data in Table 1 and formula (7) from Ref. [7], i.e. $E_H = k^{-1} \epsilon_0^{(1-k)/k} E$, one can calculate elastic moduli of the Hooke's law for tensile and compressive

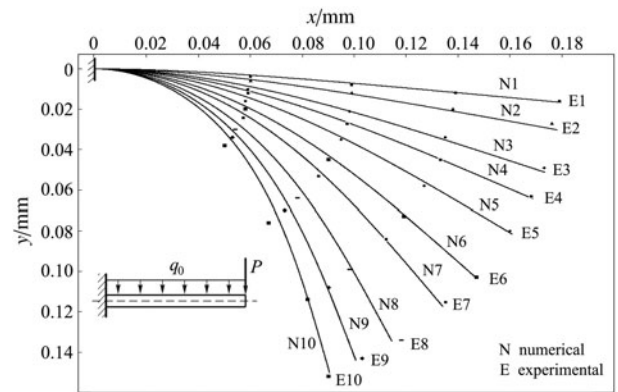


Fig. 9 Experimental and numerical results—generalized Ludwick's law

response of the material, $E_{\text{tensile}} = 14.990 \text{ N/mm}^2$ and $E_{\text{compressive}} = 14.752 \text{ N/mm}^2$. As expected, linear approximation at small strains shows considerably good agreement between experiment and calculations only for small loads, Fig. 10.

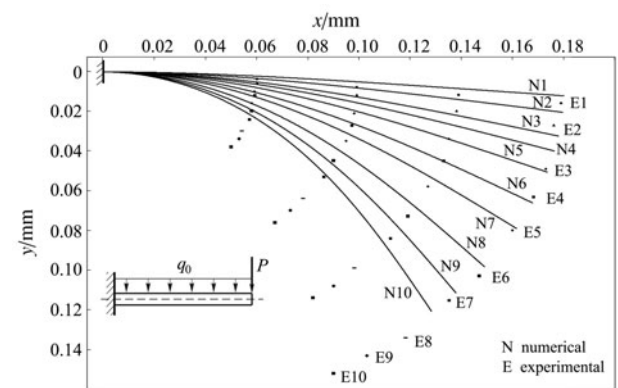


Fig. 10 Experimental and numerical results—Hooke's law

6 Conclusions

In the presented study large deflections of non-prismatic cantilever beams subjected to a combined loading which consists of a non-uniformly distributed continuous load and a concentrated load at the free end are discussed. Both geometrical and material nonlinearities are involved in this problem since the material of the cantilever is assumed to be nonlinearly elastic. A three-parametric generalized Ludwick law is used to describe the nonlinear stress–strain relationship of the material and an exact moment–curvature formula is derived for beams made from materials with different stress–strain relations in tension and compression obeying the quoted rheological law. The presented governing differential Eq. (9) is not bound to any specific loading conditions, therefore it can be applied to arbitrary loaded beams

with rectangular cross-sections. Furthermore, the generalized Ludwick law also includes the description of the behavior of both the classical Ludwick's and the Hooke's material; thus the same differential equation can also be employed for cases when Ludwick's and Hooke's elastic materials are utilized.

In this work a Runge–Kutta–Nyström integration method is used along with other numerical methods mentioned in the text to find the equilibrium states for the considered configurations of the beam. Several examples were chosen to illustrate the influence of the beam's geometry, loading conditions, and constitutive law of the material on the deflections of the beam.

In the last part of our calculations the validity of the results of the proposed solution method is verified by an experiment for a particular configuration of the beam found in Refs. [1, 2]. The experiment was carried out on a prismatic shaped beam made from a special type of vulcanized rubber which has a relatively small viscous component at smaller strains. The measured stress–strain curve of the material, which clearly indicates nonlinear behavior in both tensile and compressive domain, is modeled with the generalized Ludwick rheological model.

An excellent agreement between experimental and numerical results is obtained, indicating that the presented solution procedure is suitable for analysis of nonlinearly elastic slender beams. A linearized version of our model was tested too. As expected, it showed somewhat good agreement between experiment and calculations only for small loads.

Slightly less accurate results which are not presented in this study have also been obtained using the classical Ludwick law. Again, different nonlinear response of the material in tensile and compressive mode had to be considered; if not the numerical and experimental results would differ significantly.

Appendix

In this section of the paper we investigate the effect of the inner axial force on beam's deformation. Let us consider an extreme case and assume that the beam is subjected to a tensile axial load alone, cf. Fig. A1. The largest value of P is

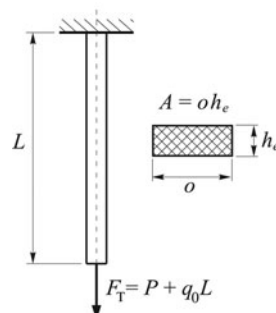


Fig. A1 Beam subjected to an axial tensile load

taken into account, which is used in our experiment and another extreme consideration, in which the entire beam's mass is concentrated at the end point.

From the following formulas, geometrical, material and load parameters, listed in Tables 1 and 4, one can calculate tensile stress

$$\begin{aligned} \sigma_T &= \frac{F_T}{A} = \frac{P + q_0L}{oh_e} \\ &= \frac{4.905 + 4.174 \times 0.180}{39.3 \times 9.8} \\ &\doteq 0.015 \text{ MPa} \end{aligned} \tag{A1}$$

and, with the help of Eq. (3) tensile strain

$$\begin{aligned} \varepsilon &= E_T^{-n} (\sigma_T + E_T \varepsilon_{0,T}^{1/n})^n - \varepsilon_{0,T}^{1/n} \\ &= 1.73^{-1.619} (0.01469 + 1.73 \times 0.001^{1/1.619})^{1.619} - 0.001 \\ &\doteq 0.00115. \end{aligned} \tag{A2}$$

Relatively small axial stress and strain values are obtained as noticed in Eqs. (A1) and (A2) even for the chosen extreme case. This strongly suggests that the influence of the inner axial force on deformation can in our case readily be neglected in comparison to the inner bending moment which dominates ($\varepsilon_T = 0.16$ and $\varepsilon_C = 0.12$) because of the geometry of the problem – slenderness of the beam.

References

- Lee, K. W.: Large deflections of cantilever beams of nonlinear elastic material under a combined loading. *Int J Nonlinear Mech* **37**, 439–443 (2002)
- Eren, I.: Determining large deflections in rectangular combined loaded cantilever beams made of non-linear Ludwick type material by means of different arc length assumptions. *Sadhana* **33**, 45–55 (2008)
- Baykara, C., Guven, U., Bayer, I.: Large deflections of a cantilever beam of nonlinear bimodulus material subjected to an end moment. *J Reinf Plast Comp* **24**, 1321–1326 (2005)
- Brojan, M., Videnic, T., Kosel, F.: Non-prismatic non-linearly elastic cantilever beams subjected to an end moment. *J Reinf Plast Comp* **26**, 1071–1082 (2007)
- Shatnawi, A.S., Al-Sadder, S.: Exact large deflection analysis of nonprismatic cantilever beams of nonlinear bimodulus material subjected to tip moment. *J Reinf Plast Comp* **26**, 1253–1268 (2007)
- Jung, J.H., Kang, T.J.: Large deflection analysis of fibers with nonlinear elastic properties. *Text Res J* **75**, 715–723 (2005)
- Brojan, M., Videnic, T., Kosel, F.: Large deflections of nonlinearly elastic non-prismatic cantilever beams made from materials obeying the generalized Ludwick constitutive law. *Meccanica* **44**, 733–739 (2009)